ACS Sustainable Chemistry & Engineering

Research Article

Cite This: ACS Sustainable Chem. Eng. 2018, 6, 11959−11967

pubs.acs.org/journal/ascecg

Analysis of the Porous Architecture and Properties of Anisotropic Nanocellulose Foams: A Novel Approach to Assess the Quality of Cellulose Nanofibrils (CNFs)

Konstantin Kriechbaum, Pierre Munier, Varvara Apostolopoulou-Kalkavoura, and Nathalie Lavoine*,†

Department of Materials and Environmental Chemistry, Stockholm University, Arrhenius Laboratory, Svante Arrhenius väg 16 C, 106 91 Stockholm, Sweden

Supporting Information

ABSTRACT: Cellulose nanofibrils (CNFs) are a unique nanomaterial because of their abundant, renewable, and biocompatible origin. Compared with synthetic nanoparticles, CNFs are commonly produced from cellulose fibers (e.g., wood pulp) by repetitive high-shear mechanical disintegration. Yet, this process is still highly demanding in energy and costly, slowing down the large-scale production and commercialization of CNFs. Reducing the energy consumption during fibers fibrillation without using any chemical or enzymatic pretreatments while sustaining the CNF quality is challenging. Here, we show that the anisotropic properties of the CNF foams are directly connected to the degree of nanofibrillation of the cellulose fibers. CNFs were produced from wood pulps using a grinder at increasing specific energy consumptions. The anisotropic CNF foams were made by directional ice templating. The porous architecture, the compressive behavior of the foams, and the CNF alignment in the foam cell walls were correlated to the degree of fibrillation. A particular value of specific energy consumption was identified with respect to the highest obtained foam properties and CNF alignment. This value indicated that the optimal degree of fibrillation, and thus CNF quality, was achieved for the studied cellulose pulp. Our approach is a straightforward tool to evaluate the CNF quality and a promising method for the benchmarking of different CNF grades.

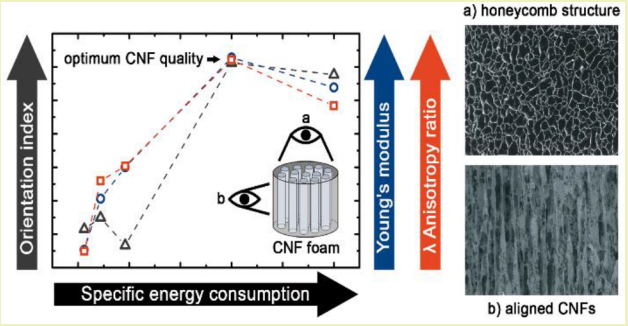

KEYWORDS: *Nanocellulose, Cellulose nanofibril, Energy consumption, Degree of fibrillation, Ice templating, Anisotropic foam*

INTRODUCTION

As an alternative to fossil-based materials, nanocellulose is the focus of intense research activities. Cellulose nanofibrils (CNFs) are one type of nanocellulose, with diameters ranging from 5 to 30 nm and aspect ratios (length/diameter) greater than 50.[1] Besides being renewable and biodegradable, CNFs combine low density with high mechanical strength, chemical inertness, and versatility.[2] The use of CNFs has been considered for a wide range of applications including composite reinforcement,[3−6] food packaging,[7,8] coatings,[9] insulation,[10−12] biomedical,[13−15] and electronic[16] applications. CNFs can be produced from any cellulose sources by successive mechanical disintegration which exposes the cellulose material to high shearing forces, thus promoting the separation of cellulose fibers into CNFs. Cost-efficient production is, however, still challenging due to high-energy consumption and processing methods which are hard to scale up.[17]

To lower the energy consumption during disintegration, enzymatic[18] or chemical[19,20] pretreatments are commonly performed prior to the mechanical treatment. However, the life cycle assessment of CNFs production shows that chemical pretreatments pose high environmental impacts due to, e.g., the use of solvents such as ethanol or isopropanol.[21] Enzymatic pretreatment and pure mechanical disintegration have similar low environmental impacts. Yet, the use of phosphate buffer and high amount of washing water contribute strongly to the terrestrial acidification and water depletion when using enzymes.[22] Lowering the environmental impact of the no-pretreatment route can be achieved by reducing the electricity usage in selecting the right equipment and running it in a sustainable manner.[21,22] Among the various mechanical treatments[23−25] reported to produce CNFs such as homogenization,[26] microfluidization,[6] and grinding,[27] the use of a grinder shows to this end various advantages: (i) the highest capacity for CNFs production, (ii) the absence of clogging caused by large fibers promoting (iii) the production of CNFs without performing any pretreatment, and (iv) the best energy efficiency.[17] Comparing the production efficiency of CNFs obtained with a grinder only is, however, more complex, as no

Received: May 18, 2018
Revised: June 29, 2018
Published: July 18, 2018

DOI: 10.1021/acssuschemeng.8b02278
ACS Sustainable Chem. Eng. 2018, 6, 11959−11967

standard protocol has been set up for a sustainable and energy-efficient production. Many different parameters influence the fibrillation outcome during grinding, such as the gap clearance between the grinding discs, the rotational speed of the lower disc, the number of grinding cycles, and the suspension concentration, volume, and viscosity. The gap clearance is commonly used as main operational parameter due to its fast and precise changeability.[28,29] Lahtinen et al.[30] used instead the total operating power as primary control parameter. Due to the thermal expansion of the grinding discs during processing, the total operating power proved to be a more reliable operating parameter than the gap clearance. However, the total operating power strongly depends on the grinder model (i.e., on the motor size and rotational speed of the grinding discs). Using the operating power surplus, namely the difference between the total and the no-load power, as main parameter to calculate the specific energy consumption is thus the most representative, yet nonstandardized way to describe and operate the grinding process.[28] Commonly, low specific energy consumptions between 1.5 and 5 kWh kg^{-1} were found to be sufficient for producing CNF films with the most improved mechanical properties.[17,31,32]

The absence of a common quality index for CNF suspensions and materials restricts, however, the comparison between the produced CNFs. There are different approaches to assess the degree of fibrillation of CNFs in the suspension state, such as determining the degree of polymerization of cellulose chains or calculating the water retention value.[33,34] The only approach to a universal quality index was recently proposed by Desmaisons et al.[32] They selected eight widely available, simple, and time-efficient criteria to characterize CNF suspensions produced using a grinder at different total energy consumptions. The focus was on the suspension properties such as the macro- and nanosized fractions, turbidity, and homogeneity but also on the indirect assessment of the structural and mechanical properties of the corresponding CNF films. The indirect evaluation of the CNF quality via film preparation gives additional information on, e.g., CNF interactions and specific surface area.[32] This approach can be argued, as no common protocol for the preparation and characterization of CNF films exists, leading to deviations in film properties and consequently to differences in resolved CNF quality.[35] In comparison to the various methods for producing CNF films, directional ice templating (or freeze-casting) of nanocellulose suspensions is a reproducible and straightforward technique to produce anisotropic CNF foams.[10,36] Processing parameters such as the freezing rate and direction during freezing of the CNF suspensions can be easily controlled, allowing for reliable and reproducible evaluation of the CNF quality.[37] CNF foams are, besides, getting more and more attention, for a wide range of applications such as biomedical scaffolds, thermal insulation, or energy storage devices,[38,39] as they combine lightweight, tunable porous structure, low thermal conductivity, and high compressive strength.[38] Assessing and optimizing the degree of fibrillation of CNFs is key for tailoring the properties of CNF foams for a target application.

Here, we investigate the properties of anisotropic CNF foams obtained by directional ice templating to evaluate the quality of CNFs. We propose a protocol allowing for an energy- and time-efficient production of CNFs, which considers the specific energy consumption as unique driving setting. The compressive strength, the porous morphology and CNF alignment in the cell walls of anisotropic freeze-cast CNF foams were quantified and correlated to the CNF fibrillation quality by combining image analysis algorithms, anisotropic thermal conductivity measurements, and X-ray diffraction analysis.

EXPERIMENTAL SECTION

Materials. Never-dried bleached Sulfite and Kraft softwood pulps were kindly provided by Domsjö Fabriker AB (Sweden) and SCA Östrand (Sweden), respectively, and used as starting materials for the CNF production. The pulps were treated with 0.5 M hydrochloric acid, ion-exchanged to sodium form using 10^{-3} M sodium bicarbonate, and washed thoroughly until neutral pH with deionized water. The cellulose, hemicelluloses, and lignin contents of the washed pulps were determined by MoRe Research (Örnsköldsvik, Sweden) and are presented in Table S1, in the Supporting Information (SI) available.

Preparation of the CNF Suspensions. Washed pulp fibers were suspended in deionized water at initial solid content of 2 wt % and dispersed for 5 min using a High-Shear Dispermix (Ystral GmbH, Germany). The suspensions were passed through a supermasscolloider grinder (model MKZA10-15J, Masuko Sangyo Co. Ltd., Japan), equipped with nonporous grinding stones containing silicon carbide (Disk model MKE 10-46#), for mechanical fibrillation. The rotational speed of the grinding stones was set to 750 rpm (25 Hz motor frequency), and the zero contact position between the two grinding stones was determined right before loading the fiber suspension. Immediately after feeding the fiber suspension into the grinder, the gap clearance between the grinding stones was set so that a certain surplus in operating power was reached. The no-load power was 3.4 kW, and the operating power during CNF production was held constant at 3.6 kW by adapting the gap clearance between −70 and −200 μm. The suspensions were circulated through the grinder and samples were taken according to prior-calculated energy consumption values.

Energy Consumption Determination. The energy consumption during grinding was determined based on the direct measurement of the operating power using a built-in three-phase wattmeter and the time of fibrillation. The specific energy consumption E_s was calculated as follows:

$$E_s[\mathrm{kWhkg^{-1}}] = \frac{P_s[\mathrm{kW}] \times t[\mathrm{h}]}{w_{\mathrm{CNF}}[\mathrm{kg}]} \quad (1)$$

where P_s is the operating power surplus, which was determined by subtracting the no-load operating power (3.4 kW) from the total operating power during grinding, t is the sampling time, and w_{CNF} is the weight of dry CNFs processed for certain time t.

Characterization of the CNF Suspensions. The morphology of the CNFs was observed by scanning electron microscopy (SEM, JEOL JSM-7401F, JEOL Ltd., Japan). A drop of 0.001 wt % CNF suspension was spread on a glass disc mounted onto a metal substrate using carbon tape, allowed to dry overnight at room temperature, and coated with a thin layer of gold. Images were recorded at an accelerating voltage of 2 kV and a working distance of 8 mm. A minimum of five images were taken for each sample at different locations to obtain a representative overview of the suspension. Diameter measurements of fibers were performed on high-magnification SEM images using the ImageJ software. The aspect ratio, A, of the CNFs was determined by sedimentation using the crowding number theory, as previously reported by Varanasi et al.[40] and Martinez et al.[41] Details on the procedure and calculations can be found in the SI. Sedimentation experiments were conducted twice per CNF suspension to ensure reproducibility.

Production of CNF Foams by Directional Ice Templating. A total of 5 g of CNF suspension at 0.5 wt % were poured into a cylindrical Teflon mold equipped with a copper bottom plate. The bottom of the mold was put in contact with dry ice, until complete freezing of the CNF suspension. The cooling rate was measured to be

DOI: 10.1021/acssuschemeng.8b02278
ACS Sustainable Chem. Eng. 2018, 6, 11959−11967

around 3 K min^{-1}. The frozen CNF suspension was then sublimated using a freeze-dryer (Alpha 1-2 LDplus, Christ, Germany) for at least 72 h at a pressure of 0.0024 mbar. Twenty foams were prepared for each CNF grade.

Characterization of the CNF Foams. The apparent density (ρ_{app}) was calculated from the mass and volume of the foams after conditioning for at least 48 h at 23 °C and 50% relative humidity (RH). The porosity (ε) was calculated as $(1 - \rho_{rel}) \times 100\%$ where ρ_{rel} is the relative density. The relative density is calculated as ρ_{app}/ρ_{skel} where ρ_{skel} is the skeletal density of cellulose (1500 kg m^{-3}).[42] Nitrogen sorption measurements were performed using an ASAP 2020 (Micromeritics Instrument Corporation, Nocross, GA, U.S.A.). The BET (Brunauer–Emmet–Teller) model was used to estimate the surface area of the foams. The CNF foams were degassed at 80 °C for 10 h prior to the measurements. The porous structure in the axial and radial directions (i.e., parallel and perpendicular to the ice crystal growth) of the CNF foams was assessed on specimens coated with a thin layer of gold using a TM 3000 SEM (Hitachi High Tech, Japan) at 5 kV accelerating voltage. The pore sizes were estimated using the ImageJ software.

The local orientation degree of the CNFs in the foam axial direction was determined by SEM image analysis using the ImageJ plug-in "OrientationJ".[43] The image analysis calculates the structure tensor of each pixel of coordinates (x; y) in its local neighborhood. The local orientation and isotropy, i.e., coherency and energy, respectively, of every pixel in the image is evaluated by computing the spatial derivatives in x and y directions using a cubic spline gradient.[44] Histograms of the local orientation weighed by the coherency were obtained for each image and they were fitted to a Gaussian function for assessing the orientation index, f. f was calculated using the full width at half-maximum (fwhm) of the Gaussians as follows:[45]

$$f = \frac{180 - \text{fwhm}}{180} \tag{2}$$

Analyses were conducted on at least ten SEM images of three different foam pieces along the axial direction.

The compressive behavior of the foams in the axial direction was evaluated using an Instron 5944 mechanical testing instrument (Instron, U.S.A.) equipped with a 500 N load cell. The foams were conditioned for at least 48 h at 23 °C and 50% relative humidity (RH) prior to the measurements. The mechanical testing was conducted at 23 °C and 50% RH at a strain rate of 10% min^{-1}. The compressive Young's modulus was determined from the slope of the initial linear region of the stress–strain curve, and the energy absorbed by the foam (i.e., toughness) was evaluated from the area under the stress–strain curve up to 70% strain. The average value and standard deviations of measurements on three to four foam specimen are reported.

X-ray diffraction (Oxford Diffraction Xcalibur 3, Agilent Technologies, U.S.A.) was used to characterize the Hermans' orientation parameter of the CNFs in the foam cell walls. Cylindrical foams were compressed parallel to the axial direction and 2D patterns were recorded with a sample-to-detector distance of 45 mm. The beam source was molybdenum (Mo $K\alpha_1$, λ = 0.71 nm), the exposure time was set at 2 × 300 s, and the CCD detector used was a Sapphire 3. The Hermans' orientation parameter, f_H, quantitatively describes the alignment of the CNFs relative to the freezing direction (i.e., axial plane).[45,46] f_H is obtained by azimuthal integration of the (200) peak of cellulose (θ = 11.4°) and the following equations:[46]

$$f_H = \frac{3(\cos^2\varphi) - 1}{2} \tag{3}$$

$$(\cos^2\varphi) = \frac{\sum_0^{\pi/2} I(\varphi)\sin\varphi\cos^2\varphi}{\sum_0^{\pi/2} I(\varphi)\sin\varphi} \tag{4}$$

where φ represents a theoretical angle between the main direction of the nanofibril and the freezing direction of the ice crystals during ice templating. This angle can be identified as the azimuthal angle on the 2D pattern. $I(\varphi)$ represents the intensity at a certain φ angle.

The axial and radial thermal conductivities (λ, mW/mK) of the anisotropic CNF foams were measured in anisotropic mode using the TPS 2500 S Thermal Constants Analyzer (Hot Disk, Sweden).[47] The heating power was set at 20 mW, and the measurement time was 10 s for each thermal conductivity measurement. The foams were enclosed in a customized cell, allowing the relative humidity (RH) to be controlled at 50% RH using a P2 humidifier (Cellkraft, Sweden). The temperature of the foams was controlled (295 K) by immersing the customized cell in a temperature controlled silicon oil bath. Five independent measurements were performed with 15 min interval time on two pairs of the investigated foams. The foams were kept at the set temperature and RH for at least 120 min prior to measurements of the thermal conductivity. The foams' density and specific heat capacity at 50% RH were given as input for performing the measurements in anisotropic mode (see SI). The thermal conductivity anisotropy ratio (AR) was calculated by dividing the axial thermal conductivity values by the radial ones.

RESULTS AND DISCUSSION

Mechanical Fibrillation via Grinding and Energy Consumption. The Kraft and Sulfite CNF suspensions were sampled at defined specific energy consumptions during grinding. We selected much lower energy consumption values than the ones reported in the literature to investigate the influence of (ultra)low energy consumption on the fibrillation quality.[17,31,32,48,49] The first three CNF suspensions, namely K1, K2, and K3 from Kraft pulp and S1, S2, and S3 from Sulfite pulp, were obtained after one, two, and three passes through the grinder. The amount of passes corresponds to specific energy consumptions of 0.12, 0.44, and 0.92 kWh kg^{-1} and 0.12, 0.39, and 0.85 kWh kg^{-1}, respectively. In addition, two CNF specimen were sampled after 3 (K4, S4) and 5 kWh kg^{-1} (K5, S5) for comparison with CNF suspensions obtained at higher energy consumption,[17] but of homogeneous and good quality, as reported by Desmaisons et al.[32] The number of passes that the suspension went through the grinder at each selected specific energy consumption is depicted in Figure 1. For the production of Sulfite CNFs the energy consumption increased with a constant rate of 0.36 kWh kg^{-1} for each pass (linear regression performed with R^2 = 0.99). The Kraft pulp,

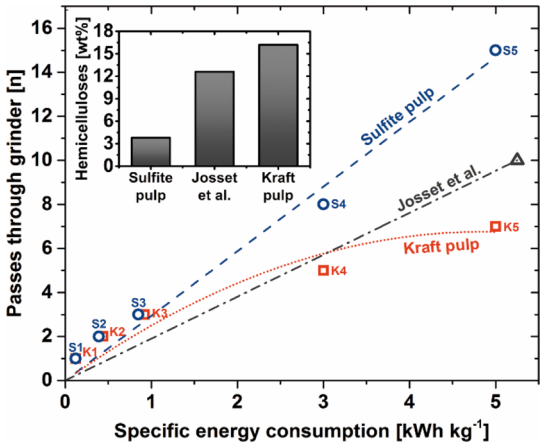

Figure 1. Correlation between the number of passes through the grinder and the specific energy consumption applied during grinding of the Kraft (orange, □) and Sulfite (blue, ○) pulps for CNF production. Data from the study of Josset et al.[26] (gray, △) is included for comparison. Inset graph: Comparison of hemicelluloses content in the three distinct pulps.

DOI: 10.1021/acssuschemeng.8b02278
ACS Sustainable Chem. Eng. 2018, 6, 11959–11967

however, required a longer grinding time per pass compared with the Sulfite pulp, which resulted in an increase in specific energy consumption for each grinding cycle (Figure 1). These results are in accordance with prior findings, showing that the presence of hemicelluloses in Kraft pulp (Table S1 in the SI) induces a better fibrillation and an increase in viscosity during grinding. Hemicelluloses act as inhibitors of the coalescence of fibrils.[50,51] For comparison, Figure 1 also reports the energy consumption and number of passes used by Josset et al.[31] for producing CNFs from bleached Kraft softwood pulp containing 12.6 wt % hemicelluloses (against 16.2 and 3.8 wt % for the Kraft and Sulfite pulps in the present case, Figure 1 inset). They reported a linear behavior between the number of passes and energy consumption, while here this correlation deviated toward higher energy input per pass for Kraft CNFs. This suggests that from a certain hemicelluloses content, the suspension viscosity increases due to promoted fibrillation, which results in a nonlinear behavior between the number of passes and the specific energy consumption of the system.

Morphology and Aspect Ratio of CNFs. The morphology and size distribution of the CNFs were qualitatively evaluated by SEM imaging. Optimal visualization of the nanofibril quality using microscopy techniques remains challenging as the whole fibrillation state cannot be accurately assessed due to, e.g., exclusion of large fibers at high magnification, or partial analysis of the CNF batches produced.[52] Due to the tight CNF entanglement, the width and length of the different materials can, besides, not be distinctively measured.[53] An overview of the fibrillation state at the different specific energy consumptions used to produce the CNFs is shown in Figure 2.

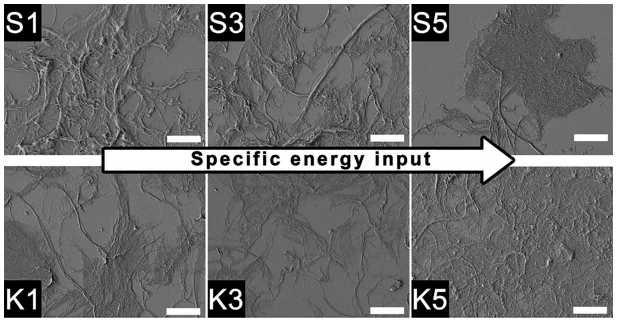

Figure 2. SEM images of CNF suspensions obtained after grinding with different specific energy input. Top row: Sulfite pulp CNFs after 0.12 (S1), 0.85 (S3), and 5 kWh kg^{-1} (S5). Bottom row: Kraft pulp CNFs after 0.12 (K1), 0.92 (K3), and 5 kWh kg^{-1} (K5). The images were taken at same magnification (×2000). The scale bar is 10 μm.

The first low energy input selected (corresponding to one pass through the grinder) was sufficient to start fibrillating both the Kraft and Sulfite pulps as shown on Figure 2 (K1 and S1). At very low specific energy consumptions (<1 kWh kg^{-1}), the Sulfite CNF suspensions still presented microfibril aggregates with diameters up to several micrometers and some short intact fibers (S1−3; S2 in Figure S1 in the SI). Higher energy input induced a more homogeneous fibrillation of the Sulfite pulp (S4−5; S4 in Figure S1 in the SI). The fibers were disintegrated into CNFs (diameters measured below 100 nm using high-magnification SEM images as shown in Figure S2 in the SI) and microfibrils up to around one micrometer in width. With a higher hemicelluloses content, the Kraft pulp disintegrated right away at early grinding stages compared with the Sulfite pulp. The presence of hemicelluloses in the pulp was reported to regulate nanofibril aggregation by hydrogen bonding and electrostatic repulsions between hemicelluloses' carboxylates, thus promoting the cell wall delamination.[32,50,51] The Kraft pulp fibers were fibrillated down to the nanofibril level (Figure S2 in the SI) with almost no residual intact fibers left, after one grinding cycle only (K1). With increasing energy input, disintegration of the pulp fibers toward nanofibrils got more homogeneous with sporadic presence of microfibrils (K2−K5, K2, and K4 in Figure S1 in the SI). Assessment of the average CNF aspect ratio was carried out by sedimentation of the Kraft and Sulfite pulps and respective CNFs (Figure 3).[40,41] Right after one grinding cycle,

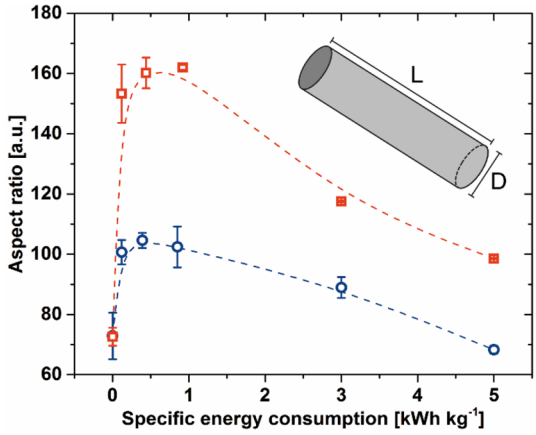

Figure 3. Evolution of the aspect ratio (L/D) of the Sulfite (blue, ○) and Kraft (orange, □) pulps and CNFs determined by sedimentation, as a function of the specific energy consumption during grinding.

we observed a steep increase in the aspect ratio of both the Sulfite and Kraft fibrillated materials (K1 and S1). This increase may result from a combination of transversal and longitudinal fibrillation of the pulp fibers when exposed to high-shear forces between grinding stones. Reduction in the fiber diameters is more probable to occur during the first grinding cycle, as it results in a drastic increase of the fibers' aspect ratio. SEM images confirm this trend showing microfibrils with much lower widths than that of the pulp fibers (K1−3 and S1−3). Additional specific energy input led to a constant average aspect ratio (K2−3 and S2−3). From 3 kWh kg^{-1}, however, a gradual decrease in aspect ratio is observed (K4−5 and S4−5) due to further transversal fibrillation. The changes in aspect ratio are more pronounced for the Kraft CNFs than the Sulfite CNFs: the aspect ratio increased by +123% between K0 (73) and K3 (162) against +40% for S0 (73) and S3 (102), respectively. This increase was followed up by a 39% decrease to 98 (K5) against a 33% decrease to 68 (S5). These results support the previous microscopic analysis and confirm that a higher content of hemicelluloses in the pulp promotes the fibrillation of the fibers to CNFs. Compared with Sulfite pulp, Kraft pulp clearly led to more energy-efficient and homogeneous fibrillated materials. This pulp has thus been selected for assessing further the fibrillation quality via the investigation of anisotropic CNF foams' properties.

Porous Architecture of the CNF Foams. Directional ice templating was carried out for producing anisotropic CNF foams, whose cell walls consist of aligned CNFs.[54] The average

DOI: 10.1021/acssuschemeng.8b02278
ACS Sustainable Chem. Eng. 2018, 6, 11959−11967

density of the foams was 5.5 ± 0.20 kg m^{-3} which resulted in a porosity of 99.63 ± 0.01%. The BET specific surface areas were in the range of 22−29 m^2 g^{-1} for all foams. Figure 4 shows SEM images of the anisotropic CNF foams' cross sections.

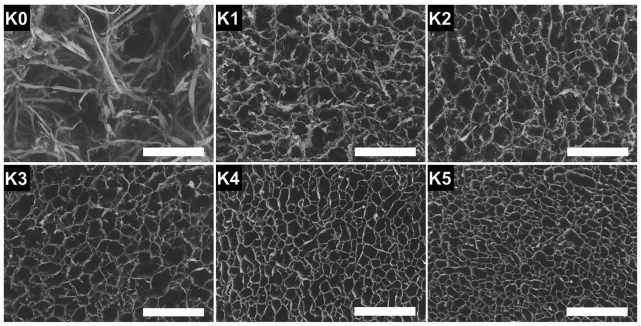

Figure 4. SEM images of the Kraft pulp (K0) and Kraft CNF (K1−5) foams' cross section. K1 to K5 CNFs were produced using a grinder at different specific energy consumption, from 0.12 (K1) to 5 kWh kg^{-1} (K5), respectively. For each image, the magnification is ×100 and the scale bar is 500 μm.

Foams prepared from the Kraft pulp showed no defined cell shape (Figure 4, K0). According to Wegst et al.,[55] two main factors determine whether freeze-cast particles are trapped inside the ice crystals or rejected and pushed aside, namely (i) the freezing front velocity and (ii) the balance between attractive and repulsive forces acting on particles. While the freezing front velocity was determined to be almost identical for all CNF suspensions (ca. 1.5 mm min^{-1}), the difference in particle engulfment should arise from the differences in forces acting on the particle. The repulsive force, F_R, that a spherical particle with a radius r experiences in the liquid phase is caused by molecular van der Waals interactions at the solid−liquid interface and can be expressed according to eq 5:[55]

$$F_R = 2\pi r \Delta\sigma_0 \left(\frac{a_0}{d}\right) \quad (5)$$

where $\Delta\sigma_0$ is the free energy of the system, d is the thickness of the liquid layer between the particle and the freezing front, and a_0 is the mean distance between molecules in this liquid layer.[55] The attractive force F_A working on the same particle is generated by the viscous drag of the moving liquid and derived from the Stokes law according to eq 6:[55]

$$F_A = \frac{6\pi\eta\nu r^2}{d} \quad (6)$$

where η is the dynamic viscosity of the liquid and ν is the freezing front velocity. After balancing those two forces and considering all parameters, except the particles' radius, constant, the repulsive and attractive forces scale both with the particles' radius. Repulsive forces directly scale with the radius, whereas attractive forces scale with the radius squared. Thus, bigger particles will be more likely attracted to the solid−liquid interface at the freezing front and consequently entrapped by the growing ice crystals. When extrapolating this theory to nonspherical particles such as fibers, the entangled fiber network observed on Figure 4-K0 therefore results from the large dimensions of the cellulose fibers. By increasing the specific energy consumption, the particle length and diameter were reduced (Figure 3), resulting in a decrease of the attractive forces between the particle (here, CNFs) and the freezing front, and in an increase in the probability for the CNFs to be rejected from the solid phase. Foams made from K1 to K5 CNF suspensions present a more defined porous structure than the K0 foam with pore sizes bigger than 30 μm, but the presence of residual macrofibrils and poorly fibrillated material in K1−3 suspensions generated defective cell boundaries and nonhomogeneous cell size distributions (Figure 4, K1 to K3). With a minimum specific energy consumption of 3 kWh kg^{-1}, the foam porous structure became significantly more homogeneous and formed a more regular and defined open honeycomb-like structure with less defective cell walls (Figure 4, K4 and K5).

Compressive Behavior of the CNF Foams. The CNF foams were compressed in the strong and stiff axial direction, i.e., in the out-of-plane deformation of the honeycombs, behaving as a cellular solid during compressive deformation.[42] The compression started with an initial cell wall bending, which is related to a linear elastic behavior and defined by an apparent Young's modulus for early stress and strain. With further compression, the collapse of the cells followed, which was shown by a plateau region of plastic deformation. For a strain range from 70 to 90%, a drastic stress increase was observed, indicating the beginning of the densification regime, i.e., when the cell walls get in contact with each other.[42] Figure 5 compares the compressive Young's modulus and energy absorption of the different CNF foams.

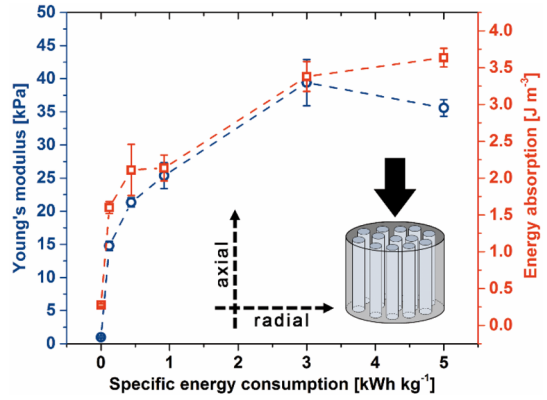

Figure 5. Influence of the specific energy consumption on the energy absorption (orange, □) and the compressive Young's modulus (blue, ○) of anisotropic CNF foams (axial compression parallel to the freezing direction, i.e., CNF alignment).

Foams made from the initial pulp fibers suspension (K0) had a very low energy absorption and almost no detectable Young's modulus resulting from the lack of fibers alignment. Owing to the honeycomb-like porous structure of the K1, K2, and K3 foams (Figure 4), a significant increase in both the energy absorption (ca. 8-fold, K3) and Young's modulus (ca. 26-fold, K3) was observed. The compressive properties of the foam improved globally with the specific energy consumption up to 3 kWh kg^{-1}. As the amount of CNFs and thus the overall share of fibers with small diameters increased with the specific energy input, more and more fibril-to-fibril bonds were formed, resulting in an entangled network that is more efficient for stress transfer and distribution.[24] The improvement in fibril interactions due to the H-bonding capacity of residual hemicelluloses also promoted the formation of a more cohesive material that better withstands external forces during compression.[51] From 3 kWh kg^{-1}, however, the energy

DOI: 10.1021/acssuschemeng.8b02278
ACS Sustainable Chem. Eng. 2018, 6, 11959−11967

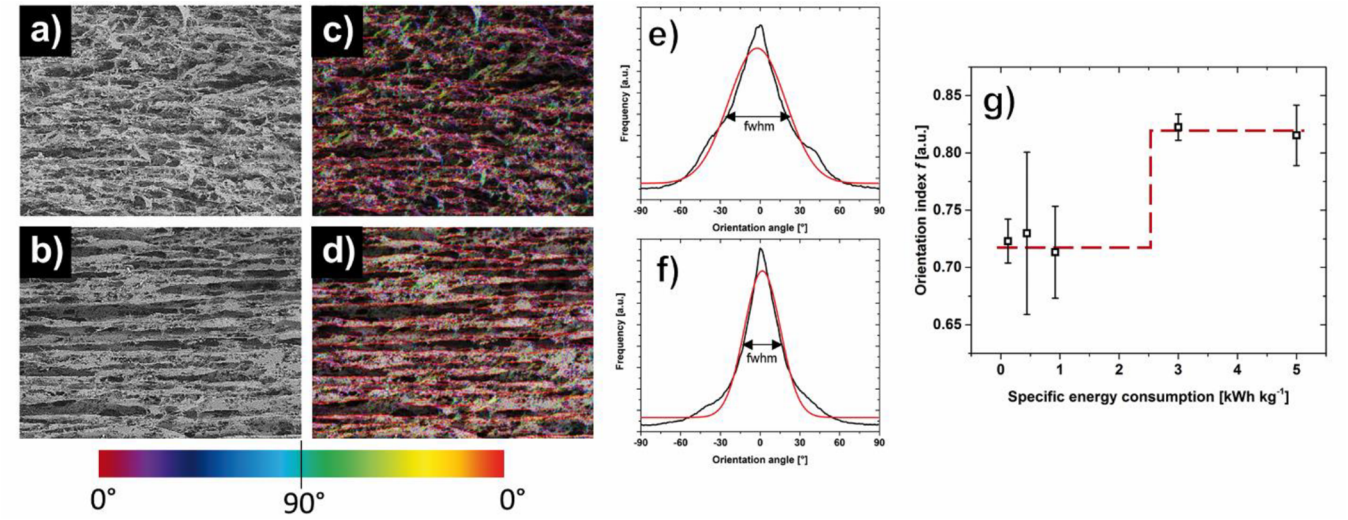

Figure 6. Quantification of the CNF alignment in the foams' cell walls by image analysis: (a,b) SEM images of the foams K1 and K4 in the axial direction, respectively, (c,d) their respective color-coded HSB maps (hue: orientation, saturation: coherency, brightness: original image), (e,f) the corresponding OrientationJ output histograms (black curve) including respective Gaussian fitting (red curve), and (g) influence of the specific energy consumption on the orientation index calculated using eq 2 for each anisotropic CNF foam.

absorption only increased by 7.5% (from K4 to K5), while the increase in energy input amounted to 67%. In the case of the Young's modulus, the plateau from 3 kWh kg^{-1} is concluded as well, as K4 and K5 foams showed similar Young's moduli, confirming the optimum value to reach for combining an energy-efficient grinding with optimal CNF foam mechanical properties.

Characterization and Quantification of the CNFs' Alignment. SEM images of the foams' longitudinal section revealed the expected oriented porous structure formed by the alignment of CNFs during freezing. The plugin OrientationJ was used to quantify the degree of local orientation observed on the SEM images. Figure 6 shows the different steps of the image analysis. Representative SEM images of K1 and K4 foams (Figure 6a,b, respectively) were selected for clear distinction between two different fibrillation states and orientation degrees of CNFs.

From the original SEM images, color-coded maps were created by the software, taking into consideration the original image brightness, the coherency as saturation and the orientation as hue setting. A higher number of red pixels illustrates a better alignment of the CNFs in the freezing direction, 0°, (horizontal direction in Figure 6), as shown Figure 6d. A greater share of green and blue color tones as observed in Figure 6c indicates CNF orientation deviating from the freezing direction. The histograms of local orientation for K1 (Figure 6e) and K4 (Figure 6f) show a peak of different width centered at 0°. The computed histograms (black curves) were fitted with a Gaussian function (red curves) to calculate the orientation index, *f*, using eq 2 (Figure 6g). The foams produced with low-energy consumption CNF suspensions (K1−3) exhibited less homogeneous and oriented cell walls than the foams produced with the K4 and K5 suspensions (Figures 4 and 6a,b). The K1, K2, and K3 foams show, indeed, a lower local orientation index with much greater standard deviations than the K4 and K5 foams (Figure 6g), which supports the SEM analysis of the foams' cross sections and the trend in mechanical properties. A higher local orientation degree is thus assessed from 3 kWh kg^{-1} in specific energy consumption, representing the minimal value to reach for achieving the highest CNF alignment (K4 and K5 foams).

The structural anisotropy of the foams can also be highlighted at a finer scale than that of the previous macroscopic attempts. One commonly reported method to estimate the alignment of rod-like particles is X-ray diffraction.[36,45] During freeze-casting, the shear forces induced by the ice crystals growth and the resulting confinement cause the fibrils to pack, to a certain extent, parallel to the freezing direction. Quantifying the orientation of the cellulose crystal units along the freezing direction using X-ray diffraction may be another tool to assess the fibrillation quality of the CNF suspensions. The Hermans' orientation parameter, f_H, quantifies the crystals alignment (eq 3). The closer f_H is to 1, the more the crystal units of the CNFs are aligned. f_H was calculated for the foams K0 to K5 (Figure S3 in the SI). K0 displays a value of $f_H = 0.01$, which in theory corresponds to a completely random distribution,[46] meaning that the shear forces were insufficient to induce any orientation during freezing. All of the other CNF foams, in comparison, have f_H values ranging between 0.20 and 0.31, indicating a moderate alignment. To put these values into perspective, they are within the same range as values obtained for drawn films of regenerated cellulose (up to $f_H = 0.29$)[56] and are much lower than the coefficients calculated for drawn films made of TEMPO-oxidized CNFs ($f_H = 0.34$ to 0.72),[45] which is to be expected given the particles' sizes. It is however difficult to state that f_H allows for an effective discrimination in the fibrillation degree, considering the similarity between the values obtained for K3 and K5 and the low value of K4. Because the mechanically treated CNF suspensions did not show any significant differences in f_H values, XRD is in the present case not the optimal experimental tool for assessing the fibrillation quality. However, when considering previous studies reporting clear differences in f_H values between, e.g., TEMPO−CNFs and regenerated cellulose,[45,56] determining the f_H orientation parameter can be a satisfactory tool to estimate the fiber orientation degree at the single fibril level. The use of f_H seems more appropriate for comparing different systems (e.g., different types of CNFs or processing) than for

DOI: 10.1021/acssuschemeng.8b02278
ACS Sustainable Chem. Eng. 2018, 6, 11959−11967

tracking the evolution of a single system over the course of one processing method. In the present case, assessing the macroscopic properties of the foams is more reliable to evaluate the fibrillation quality of the CNFs.

The foams' thermal conductivity was evaluated as another indirect method to quantify the CNF alignment in the foams in correlation with the fibrillation quality. The thermal conductivity at room temperature of CNF foams with cell sizes below 1 mm is dependent on two main contributions, (i) the solid contribution related to the heat conduction in the cell walls and (ii) the gas contribution corresponding to the conduction of air in the macropores.[57−59] Evaluation of the anisotropy of the CNF foams was conducted via the measurement of the thermal conductivity in axial and radial directions. Figure 7a shows the axial and radial thermal conductivity values of the different CNF foams determined at 50% relative humidity and 22 °C.

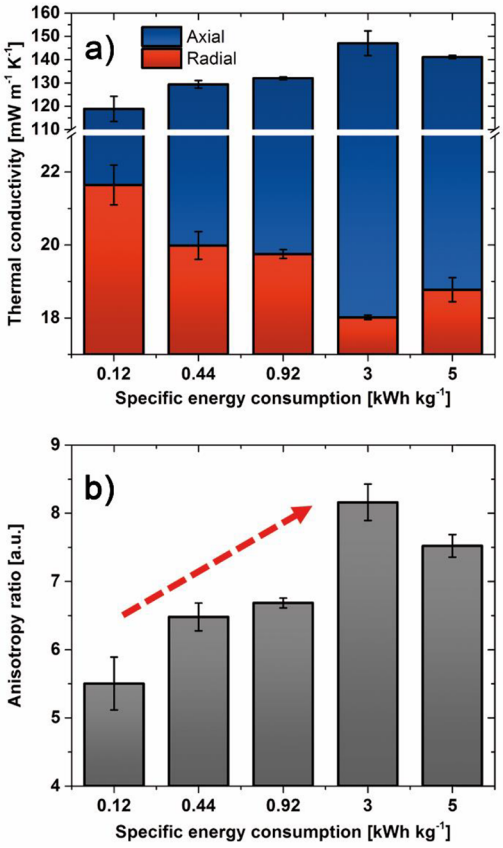

Figure 7. Thermal conductivity of anisotropic CNF foams: an indirect quantitative method of the CNF alignment. (a) Axial (blue) and radial (orange) thermal conductivity of the foams measured at 50% RH and 22 °C. (b) Anisotropy ratio of thermal conductivity defined as the ratio of the axial by the radial thermal conductivity values. Anisotropy values greater than 1 indicate CNF alignment in the axial direction.

As previously reported,[10] the axial thermal conductivity of anisotropic CNF foams is significantly higher than the radial one due to an important solid contribution of the cell walls in the axial direction. Previous studies have indeed shown that the gas conduction inside macroporous solids is very close to the gaseous conduction in free space (25 mW m^{-1} K^{-1}) and cannot account for the significantly higher axial thermal conductivity.[60] The axial thermal conductivity increased with the increasing specific energy input from 119 to 132 mW m^{-1} K^{-1} (K1 to K3) and leveled off around 147 ± 5 mW m^{-1} K^{-1} from 3 kWh kg^{-1} (K4−5). The opposite trend was observed for the radial thermal conductivity. It is worth noting that each CNF foam behaves as a superinsulating material in the radial direction (i.e., thermal conductivity, $\lambda < \lambda_{air}$ = 25 mW m^{-1} K^{-1}).[10] When calculating the anisotropy ratio (Figure 7b), an increase in the anisotropy is observed up to 3 kWh kg^{-1}. The CNFs obtained with a higher specific energy input resulted in more anisotropic structures, which can be compared to the structure of TEMPO-oxidized CNF (T-CNF) foams made by freeze-casting.[10,36] Wicklein et al.[10] reported an axial and radial thermal conductivity of 150 and 18 mW m^{-1} K^{-1}, respectively, for T-CNF foams at 50% RH and 22 °C. These values are similar to those measured for the foam K4 made from the CNF suspension produced with a specific energy consumption of 3 kWh kg^{-1}. T-CNFs are produced from a combination of chemical and mechanical treatments, which usually results in the most fibrillated CNF materials, reaching a nanofibril width down to 3−4 nm.[20] This level of fibrillation has so far never been achieved by mechanical disintegration only. Yet, in this study, we obtained CNF foams exhibiting very similar thermal conductivities to that of T-CNF foams, by solely using a mechanical fibrillation and without achieving CNFs of 3−4 nm in width.

Figure 8 summarizes the correlations observed between the CNF alignment and the mechanical and thermal properties of

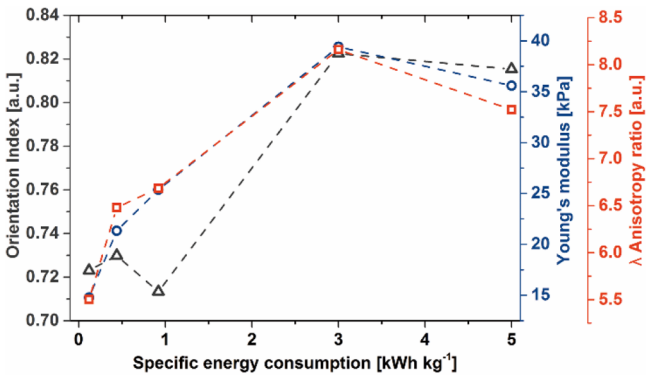

Figure 8. Correlation between the degree of fibrillation set by the specific energy consumption during grinding and the properties of the anisotropic CNF foams, namely the CNF orientation index (gray, △), the compressive Young's modulus (blue, ○), and the anisotropy ratio of thermal conductivity (orange, □).

the Kraft CNF foams as a function of the specific energy consumption used to produce the CNFs. Each properties optimum converges to a specific energy consumption of 3 kWh kg^{-1}, which is the optimum value to reach for producing the best CNF fibrillation quality by energy-efficient grinding.

CONCLUSION

Kraft and Sulfite pulps were successfully fibrillated using the operating energy input surplus as the main processing parameter during grinding. The presence of residual hemicelluloses in the Kraft pulp promoted the energy-efficient disintegration of the cellulose fibers into CNFs and led to the production of a more homogeneous material in size. The characterization of the CNF aspect ratio by sedimentation resulted in a first overview of the degree of nanofibrillation.

DOI: 10.1021/acssuschemeng.8b02278
ACS Sustainable Chem. Eng. 2018, 6, 11959−11967

The analysis of the anisotropic properties of the Kraft CNF foams prepared by directional ice templating was presented as a novel approach to assess quantitatively the fibrillation quality of the CNFs. The macroporous morphology and the compressive behavior of the CNF foams revealed a uniform porous honeycomb structure and optimal compressive Young's modulus and toughness at an energy consumption of 3 kWh kg^{-1}. The study of the CNF alignment in the foam cell walls via novel techniques such as image analysis and thermal conductivity measurement confirmed the optimal plateau at 3 kWh kg^{-1}. Correlating the properties of anisotropic CNF foams with the degree of fibrillation of the CNFs is a reproducible, direct, and promising approach, which paves the way for energy-efficient production of CNFs without compromising the quality of the suspension.

■ ASSOCIATED CONTENT

Supporting Information

The Supporting Information is available free of charge on the ACS Publications website at DOI: 10.1021/acssuschemeng.8b02278.

Additional information on materials and methods as well as SEM images of the CNFs and quantification of CNF alignment (PDF)

■ AUTHOR INFORMATION

Corresponding Author

*Tel: +1 919 513 3235. E-mail: nmlavoin@ncsu.edu.

ORCID

Konstantin Kriechbaum: 0000-0002-3737-5303

Nathalie Lavoine: 0000-0002-8259-4070

Present Address

[†]Department of Forest Biomaterials, College of Natural Resources, North Carolina State University, 2820 Faucette Dr., Raleigh, NC 27695, U.S.A.

Author Contributions

The manuscript was written through contributions of all authors. All authors have given approval to the final version of the manuscript.

Notes

The authors declare no competing financial interest.

■ ACKNOWLEDGMENTS

The authors acknowledge the Swedish Research Council for Environment, Agricultural Sciences and Spatial Planning, the Swedish Energy Agency (Energimyndigheten), the Swedish Foundation for strategic research (SSF), and the Marie Sklodowska-Curie Actions Innovative Training Networks (H2020-MSCA-ITN-2014) for financial support. The authors would especially like to thank Prof. Lennart Bergström for his support and Prof. Aji Mathew for her fruitful advice.

■ REFERENCES

(1) Mariano, M.; El Kissi, N.; Dufresne, A. Cellulose Nanocrystals and Related Nanocomposites: Review of Some Properties and Challenges. *J. Polym. Sci., Part B: Polym. Phys.* **2014**, *52* (12), 791–806.

(2) Abitbol, T.; Rivkin, A.; Cao, Y.; Nevo, Y.; Abraham, E.; Ben-Shalom, T.; Lapidot, S.; Shoseyov, O. Nanocellulose, a Tiny Fiber with Huge Applications. *Curr. Opin. Biotechnol.* **2016**, *39*, 76–88.

(3) Dufresne, A. Polysaccharide Nano Crystal Reinforced Nanocomposites. *Can. J. Chem.* **2008**, *86* (6), 484–494.

(4) Siró, I.; Plackett, D. Microfibrillated Cellulose and New Nanocomposite Materials: A Review. *Cellulose* **2010**, *17* (3), 459–494.

(5) Klemm, D.; Kramer, F.; Moritz, S.; Lindström, T.; Ankerfors, M.; Gray, D.; Dorris, A. Nanocelluloses: A New Family of Nature-Based Materials. *Angew. Chem., Int. Ed.* **2011**, *50* (24), 5438–5466.

(6) Siqueira, G.; Bras, J.; Dufresne, A. Cellulosic Bionanocomposites: A Review of Preparation, Properties and Applications. *Polymers (Basel, Switz.)* **2010**, *2* (4), 728–765.

(7) Li, F.; Mascheroni, E.; Piergiovanni, L. The Potential of Nanocellulose in the Packaging Field: A Review. *Packag. Technol. Sci.* **2015**, *28* (6), 475–508.

(8) Serpa, A.; Velásquez-Cock, J.; Gañán, P.; Castro, C.; Vélez, L.; Zuluaga, R. Vegetable Nanocellulose in Food Science: A Review. *Food Hydrocoll.* **2016**, *57*, 178–186.

(9) Brodin, F. W.; Gregersen, O. W.; Syverud, K. Cellulose Nanofibrils: Challenges and Possibilities as a Paper Additive or Coating Material - a Review. *Nord. Pulp Pap. Res. J.* **2014**, *29* (1), 156–166.

(10) Wicklein, B.; Kocjan, A.; Salazar-Alvarez, G.; Carosio, F.; Camino, G.; Antonietti, M.; Bergström, L. Thermally Insulating and Fire-Retardant Lightweight Anisotropic Foams Based on Nanocellulose and Graphene Oxide. *Nat. Nanotechnol.* **2015**, *10*, 277–283.

(11) Kobayashi, Y.; Saito, T.; Isogai, A. Aerogels with 3D Ordered Nanofiber Skeletons of Liquid-Crystalline Nanocellulose Derivatives as Tough and Transparent Insulators. *Angew. Chem., Int. Ed.* **2014**, *53* (39), 10394–10397.

(12) Yildirim, N.; Shaler, S. M.; Gardner, D. J.; Rice, R.; Bousfield, D. W. Cellulose Nanofibril (CNF) Reinforced Starch Insulating Foams. *Cellulose* **2014**, *21* (6), 4337–4347.

(13) Gatenholm, P.; Klemm, D. Bacterial Nanocellulose as a Renewable Material for Biomedical Applications. *MRS Bull.* **2010**, *35* (3), 208–213.

(14) Jorfi, M.; Foster, E. J. Recent Advances in Nanocellulose for Biomedical Applications. *J. Appl. Polym. Sci.* **2015**, *132* (14), n/a.

(15) Sultan, S.; Mathew, A. 3D Printed Scaffolds with Gradient Porosity Based on Cellulose Nanocrystal Hydrogel. *Nanoscale* **2018**, *10*, 4421–4431.

(16) Hoeng, F.; Denneulin, A.; Bras, J. Use of Nanocellulose in Printed Electronics: A Review. *Nanoscale* **2016**, *8* (27), 13131–13154.

(17) Spence, K. L.; Venditti, R. A.; Rojas, O. J.; Habibi, Y.; Pawlak, J. J. A Comparative Study of Energy Consumption and Physical Properties of Microfibrillated Cellulose Produced by Different Processing Methods. *Cellulose* **2011**, *18* (4), 1097–1111.

(18) Henriksson, M.; Henriksson, G.; Berglund, L. A.; Lindström, T. An Environmentally Friendly Method for Enzyme-Assisted Preparation of Microfibrillated Cellulose (MFC) Nanofibers. *Eur. Polym. J.* **2007**, *43* (8), 3434–3441.

(19) Aulin, C. *Novel Oil Resistant Cellulosic Materials*; Ph.D. Thesis; KTH Royal Institute of Technology: Stockholm, Sweden, 2009.

(20) Saito, T.; Kimura, S.; Nishiyama, Y.; Isogai, A. Cellulose Nanofibers Prepared by TEMPO-Mediated Oxidation of Native Cellulose. *Biomacromolecules* **2007**, *8* (8), 2485–2491.

(21) Li, Q.; McGinnis, S.; Sydnor, C.; Wong, A.; Renneckar, S. Nanocellulose Life Cycle Assessment. *ACS Sustainable Chem. Eng.* **2013**, *1* (8), 919–928.

(22) Arvidsson, R.; Nguyen, D.; Svanström, M. Life Cycle Assessment of Cellulose Nanofibrils Production by Mechanical Treatment and Two Different Pretreatment Processes. *Environ. Sci. Technol.* **2015**, *49* (11), 6881–6890.

(23) Li, Q.; Renneckar, S. Molecularly Thin Nanoparticles from Cellulose: Isolation of Sub-Microfibrillar Structures. *Cellulose* **2009**, *16* (6), 1025–1032.

(24) Dufresne, A.; Cavaille, J.-Y.; Vignon, M. R. Mechanical Behavior of Sheets Prepared from Sugar Beet Cellulose Microfibrils. *J. Appl. Polym. Sci.* **1997**, *64* (6), 1185–1194.

(25) Zhang, L.; Tsuzuki, T.; Wang, X. Preparation of Cellulose Nanofiber from Softwood Pulp by Ball Milling. *Cellulose* **2015**, *22* (3), 1729−1741.
(26) Turbak, A. F.; Snyder, F. W.; Sandberg, K. R. Suspensions Containing Microfibrillated Cellulose, U.S. Patent US4500546A, 1985.
(27) Iwamoto, S.; Nakagaito, A. N.; Yano, H. Nano-Fibrillation of Pulp Fibers for the Processing of Transparent Nanocomposites. *Appl. Phys. A: Mater. Sci. Process.* **2007**, *89* (2), 461−466.
(28) Kang, T.; Paulapuro, H. New Mechanical Treatment for Chemical Pulp. *Proc. Inst. Mech. Eng., Part E* **2006**, *220* (3), 161−166.
(29) Hu, C.; Zhao, Y.; Li, K.; Zhu, J. Y.; Gleisner, R. Optimizing Cellulose Fibrillation for the Production of Cellulose Nanofibrils by a Disk Grinder. *Holzforschung* **2015**, *69* (8), 993−1000.
(30) Lahtinen, P.; Liukkonen, S.; Pere, J.; Sneck, A.; Kangas, H. A Comparative Study of Fibrillated Fibers from Different Mechanical and Chemical Pulps. *BioResources* **2014**, *9* (2), 2115−2127.
(31) Josset, S.; Orsolini, P.; Siqueira, G.; Tejado, A.; Tingaut, P.; Zimmermann, T. Energy Consumption of the Nanofibrillation of Bleached Pulp, Wheat Straw and Recycled Newspaper through a Grinding Process. *Nord. Pulp Pap. Res. J.* **2014**, *29* (1), 167−175.
(32) Desmaisons, J.; Boutonnet, E.; Rueff, M.; Dufresne, A.; Bras, J. A New Quality Index for Benchmarking of Different Cellulose Nanofibrils. *Carbohydr. Polym.* **2017**, *174*, 318−329.
(33) Qin, Y.; Qiu, X.; Zhu, J. Y. Understanding Longitudinal Wood Fiber Ultra-Structure for Producing Cellulose Nanofibrils Using Disk Milling with Diluted Acid Prehydrolysis. *Sci. Rep.* **2016**, *6*, 1−12.
(34) Gu, F.; Wang, W.; Cai, Z.; Xue, F.; Jin, Y.; Zhu, J. Y. Water Retention Value for Characterizing Fibrillation Degree of Cellulosic Fibers at Micro and Nanometer Scales. *Cellulose* **2018**, *25* (5), 2861−2871.
(35) Hervy, M.; Santmarti, A.; Lahtinen, P.; Tammelin, T.; Lee, K.-Y. Sample Geometry Dependency on the Measured Tensile Properties of Cellulose Nanopapers. *Mater. Des.* **2017**, *121*, 421−429.
(36) Munier, P.; Gordeyeva, K.; Bergström, L.; Fall, A. B. Directional Freezing of Nanocellulose Dispersions Aligns the Rod- Like Particles and Produces Low-Density and Robust Particle Networks. *Biomacromolecules* **2016**, *17* (5), 1875−1881.
(37) Deville, S. Freeze-Casting of Porous Biomaterials: Structure, Properties and Opportunities. *Materials* **2010**, *3* (3), 1913−1927.
(38) Lavoine, N.; Bergström, L. Nanocellulose-Based Foams and Aerogels: Processing, Properties, and Applications. *J. Mater. Chem. A* **2017**, *5* (31), 16105−16117.
(39) De France, K. J.; Hoare, T.; Cranston, E. D. Review of Hydrogels and Aerogels Containing Nanocellulose. *Chem. Mater.* **2017**, *29* (11), 4609−4631.
(40) Varanasi, S.; He, R.; Batchelor, W. Estimation of Cellulose Nanofibre Aspect Ratio from Measurements of Fibre Suspension Gel Point. *Cellulose* **2013**, *20* (4), 1885−1896.
(41) Martinez, D. M.; Buckley, K.; Jivan, S.; Lindstrom, A.; Thiruvengadaswamy, R.; Olson, J. A.; Ruth, T. J.; Kerekes, R. J. Characterizing the Mobility of Papermaking Fibres during Sedimentation. In *Proceedings of the Transactions of 12th fundamental Research Symposium*; Oxford: Oxford, U.K., 2001; pp 225−254.
(42) Gibson, L. J.; Ashby, M. F. *Cellular Solids: Structure and Properties*; Cambridge University Press: Cambridge, U.K., 1999.
(43) Rezakhaniha, R.; Agianniotis, A.; Schrauwen, J. T. C.; Griffa, A.; Sage, D.; Bouten, C. V. C.; Van De Vosse, F. N.; Unser, M.; Stergiopulos, N. Experimental Investigation of Collagen Waviness and Orientation in the Arterial Adventitia Using Confocal Laser Scanning Microscopy. *Biomech. Model. Mechanobiol.* **2012**, *11* (3−4), 461−473.
(44) Püspöki, Z.; Storath, M.; Sage, D.; Unser, M. *Adv. Anat., Embryol. Cell Biol.*; Springer: Berlin, 2016; Vol. *219*, pp 69−93.
(45) Sehaqui, H.; Ezekiel Mushi, N.; Morimune, S.; Salajkova, M.; Nishino, T.; Berglund, L. A. Cellulose Nanofiber Orientation in Nanopaper and Nanocomposites by Cold Drawing. *ACS Appl. Mater. Interfaces* **2012**, *4* (2), 1043−1049.
(46) Hermans, J. J.; Hermans, P. H.; Vermaas, D.; Weidinger, A. Quantitative Evaluation of Orientation in Cellulose Fibres from the X-Ray Fibre Diagram. *Recl. des Trav. Chim. des Pays-Bas* **1946**, *65* (6), 427−447.
(47) Apostolopoulou-Kalkavoura, V.; Gordeyeva, K.; Lavoine, N.; Bergström, L. Thermal Conductivity of Hygroscopic Foams Based on Cellulose Nanofibrils and a Nonionic Polyoxamer. *Cellulose* **2018**, *25* (2), 1117−1126.
(48) Wang, Q. Q.; Zhu, J. Y.; Gleisner, R.; Kuster, T. A.; Baxa, U.; McNeil, S. E. Morphological Development of Cellulose Fibrils of a Bleached Eucalyptus Pulp by Mechanical Fibrillation. *Cellulose* **2012**, *19* (5), 1631−1643.
(49) Jonoobi, M.; Mathew, A. P.; Oksman, K. Producing Low-Cost Cellulose Nanofiber from Sludge as New Source of Raw Materials. *Ind. Crops Prod.* **2012**, *40*, 232−238.
(50) Solala, I.; Volperts, A.; Andersone, A.; Dizhbite, T.; Mironova-Ulmane, N.; Vehniäinen, A.; Pere, J.; Vuorinen, T. Mechanoradical Formation and Its Effects on Birch Kraft Pulp during the Preparation of Nanofibrillated Cellulose with Masuko Refining. *Holzforschung* **2012**, *66* (4), 477−483.
(51) Iwamoto, S.; Abe, K.; Yano, H. The Effect of Hemicelluloses on Wood Pulp Nanofibrillation and Nanofiber Network Characteristics. *Biomacromolecules* **2008**, *9* (3), 1022−1026.
(52) Chinga-Carrasco, G. Optical Methods for the Quantification of the Fibrillation Degree of Bleached MFC Materials. *Micron* **2013**, *48*, 42−48.
(53) Henriksson, M.; Berglund, L. A.; Isaksson, P.; Lindström, T.; Nishino, T. Cellulose Nanopaper Structures of High Toughness. *Biomacromolecules* **2008**, *9* (6), 1579−1585.
(54) Deville, S.; Saiz, E.; Nalla, R. K.; Tomsia, A. P. Freezing as a Path to Build Complex Composites. *Science (Washington, DC, U. S.)* **2006**, *311* (5760), 515−518.
(55) Wegst, U. G. K.; Schecter, M.; Donius, A. E.; Hunger, P. M. Biomaterials by Freeze Casting. *Philos. Trans. R. Soc., A* **2010**, *368* (1917), 2099−2121.
(56) Gindl, W.; Keckes, J. Drawing of Self-Reinforced Cellulose Films. *J. Appl. Polym. Sci.* **2007**, *103* (4), 2703−2708.
(57) Glicksman, L. R. Heat Transfer in Foams. In *Low density cellular plastics*; Hilyard, N. C., Cunningham, A., Eds.; Springer: Dordrecht, The Netherlands, 1994; pp 104−152.
(58) Collishaw, P. G.; Evans, J. R. G. An Assessment of Expressions for the Apparent Thermal-Conductivity of Cellular Materials. *J. Mater. Sci.* **1994**, *29* (9), 2261−2273.
(59) Berge, A.; Johansson, P. Ä. R. *Literature Review of High Performance Thermal Insulation*; Chalmers University of Technology: Göteborg, Sweden, 2012.
(60) Zeng, S. Q.; Hunt, A.; Greif, R. Transport Properties of Gas in Silica Aerogel. *J. Non-Cryst. Solids* **1995**, *186*, 264−270.

DOI: 10.1021/acssuschemeng.8b02278
ACS Sustainable Chem. Eng. 2018, 6, 11959−11967